PTV measurement of drag coefficient of fibrous particles with large aspect ratio

Guo Q. QI, Graham J. NATHAN and Richard M. KELSO

School of Mechanical Engineering and Centre for Energy Technology, The University of Adelaide, Adelaide SA 5005 AUSTRALIA

Email: guo.qi@adelaide.edu.au

Abstract

The aerodynamic behaviour of long aspect ratio nylon fibrous particles has been investigated experimentally whilst settling in air under super dilute conditions without any influence of secondary flows and at fibre Reynolds numbers of 0.5 - 2 based on fibre diameter. A method for laser-based measurement of the orientations and velocities of fibrous particles is presented. The experimental apparatus employs a two-dimensional Particle Tracking Velocimetry (PTV) to calculate orientation and velocity based on the two end-points. The controlling length scale in the relationship between Reynolds number and drag coefficient was investigated and the equivalent diameter of settling fibre in air was reported.

Keywords: Sedimentation; aerodynamics; PTV; fibrous particle; drag coefficient

1 Introduction

A fibrous particle settling in air under the influence of gravity will accelerate until the gravitational force is exactly balanced by the drag force, because the buoyancy can be ignored in this case. The constant velocity reached is called terminal settling velocity. The terminal settling velocity of a fibre is strongly influenced by its orientation[16]. Although research has been conducted on the problem of drag for cylindrical particle, it seems that no experimental investigations have been undertaken to determine its equivalent diameter of

settling fibre in air with large aspect ratio to assess its aerodynamic behaviour.

Fan *et al* [1] experimentally studied the relationship between drag coefficient (C_D) of slender particles with large aspect ratio (L/d=4-37) and Re_d (0.4-100). They proposed following equation to calculate drag coefficient, which needs to be assessed.

$$C_D = \frac{1}{\sin\theta}\left(\frac{\rho_{fp}}{\rho_f}\right)^{-1.537}\left[\frac{d^3(\rho_{fp}-\rho_f)^2 g}{\mu^2}\right]^{0.8524}\frac{24}{\mathrm{Re}_d}(0.006983+0.6224\,\mathrm{Re}_d^{-1.046}) \qquad (1)$$

Here θ is the orientation of the fibre, which is the angle between the major axis of the fibre and the direction of the gravity; ρ_{fp} and ρ_f are the fibre and fluid density respectively; d is the diameter of the fibre and μ is the viscosity of fluid; $Re_d = \rho_{air} V_{fp} d/\mu$.

Clift *et al* [2] reported that for a single fibrous particle with Reynolds number $Re_d > 0.01$, a cylinder falls with its axis oriented horizontally and exhibits steady motion with this orientation up to Re_d of order 100. However, this is yet to be extended to a cloud of interacting particles in suspension. Also Clift proposed the following model to calculate C_D of a cylindrical particle:

$$C_D = 9.689(\mathrm{Re}_d)^{-0.78} + 1.42(\mathrm{Re}_d)^{0.04} \quad (0.1 < Re_d < 5) \qquad (2)$$

Sphericity, ψ, is a measure of how closely a particle conform to a spherical shape. It is widely used in the study of non-spherical particle and has also been used to evaluate fibrous particles. Sphericity was defined to be:

$$\psi = \frac{A_s}{A_p} \qquad (3)$$

where A_s is the surface area of sphere that has the same volume as the non-spherical particle and A_p is the surface area of the non-spherical particle. Based on this definition, the

sphericity of a cylindrical particle becomes:

$$\psi_{fp} = \frac{d_{ev}^{\ 2}}{dL + d^2/2} \qquad (4)$$

where d_{ev} is the diameter of the sphere that has the same volume as the fibrous particle, e.g. equivalent volume diameter, and d and L are the diameter and length of the fibrous particle respectively. For present fibre, ψ =0.38.

Haider and Levenspiel [3] proposed the following four parameters correlation to calculate $C_{D.}$

$$C_D = \frac{24}{\mathrm{Re}}(1 + A\,\mathrm{Re}^B) + \frac{C}{1 + \frac{D}{\mathrm{Re}}} \qquad (5)$$

Where the values of *A,B,C,D* are functions of ψ. The authors pointed out that, while the fit is quite good for isometric particles, $\psi > 0.67$, it is poorer outside this range. They also argued that "for close to isometrically shaped particles, those with no one very much longer or very much shorter dimension, the sphericity is a useful measure, most likely the best single parameter for describing the shape for falling particles." That is, Eq (5) is not expected to be appropriate for a fibrous particle with a long aspect ratio. Furthermore particles with entirely different shapes and different aerodynamic behaviour can have the same sphericity. For example, a disc particle and a fibrous particle can have the same Ψ, but have a totally different aerodynamic behaviour. Therefore, more work is needed to develop relationships that characterize drag for long aspect ratio fibres.

Venu Maddhav and Chhabra [4] investigated cylinders settling in a confined environment. The settling cylinders were observed to retain their initial orientation during settling, which is opposite to the conclusion of Clift *et al* [2] for a single fibre. Under the conditions of 0.01

< Re < 400, 0.35 < Ψ < 0.7 and 0.05 < L/d < 50, Venu Maddhav and Chhabra [4] developed the following expression to calculate C_D:

$$C_D = \frac{24}{\mathrm{Re}}(1 + 0.604\,\mathrm{Re}^{0.529}) \qquad (6)$$

However the terminal settling velocity with the above range of Re, the cylinder falls with its axis oriented horizontally [2]. Therefore it doubtful that the findings of Venu Maddhav and Chhabra [4] can be extrapolated to an unconfined environment in which the orientation is not generally horizontal.

In addition to above investigations on cylindrical particles, numerous studies have been conducted by employing equal volume diameter and sphericity to investigate C_D of non-spherical particles [8]-[15]. Based on the work of Haider and Levenspiel [3], Ganser [5] introduced two shape factors to a drag correlation. But like Haider's work, for particles where ψ<0.5, Ganser's work is applicable to disk only. Swamee and Ojha [6] also developed a correlation with the Corey shape factor, $\beta = c/(ab)^{1/2}$, where $a>b>c$ are the lengths of the three principal axis of the particle. However this parameter is only applicable in the range of 0.3 < β <1, making it unsuitable for long aspect ratio fibres such as those considered here. For present fibre Corey shape factor is 0.16, so it is not applicable.

In the light of the previous investigations described above, we seek to further the understanding of the aerodynamics of settling long fibrous particles in the range of Re_d = 0.5 – 2, with a high density ratio of particle to fluid and no boundary limitation. Furthermore we would investigate the equivalent diameter of a fibre with large aspect ratio settling in air. As can be seen from the literature review this equivalent diameter has yet to be reported previously. Therefore, the first aim of present work is to develop a novel method to measure the velocity and orientation of a fibrous particle simultaneously. The second aim is to employ

this method to obtain the relationship (equations) between a fibre's number density and its settling velocity in the super dilute regime. The third aim is to investigate the equivalent diameter that suit the fibre with large aspect ratio and drag coefficient and assess the two models proposed by previous investigators.

2 Experimental apparatus/facility

2.1 Measurement technique and set-up of PTV system

Fig. 1 presents a schematic diagram of experimental apparatus. To avoid any influence of electrostatics, the pipe was earthed. The experimental method employed a typical Particle Tracking Velocimetry (PTV) technique. The laser was operated in a pulsed mode and the camera in a two-frame mode. The laser sheet was formed by telescopic and diverging lenses. The settling fibrous particles were illuminated by the laser sheet at regular intervals of time and the CCD camera used to record two images of the fibres separated by a delay of about 2.5 ms. The oscilloscope and delay generator were employed in the experiments. The oscilloscope was used to monitor and validate the time separation chosen for the experiments. A DG-535 delay generator was employed to trigger both the laser flash-lamps and the camera. The laser used in the experiments was a Quantel Brilliant Twins double-cavity pulsed Nd: YAG 10 Hz laser, frequency doubled to provide a wavelength of 532nm. The output energy of laser head was set to provide either 250 mJ/pulse or 400 mJ/pulse. The camera was a Kodak MegaPlus ES1.0 with a CCD array of 1008pixels × 1018pixels. The resolution was around 26 μm/pixel and the viewing area was 26mm× 26 mm. Xcap software was used as the operating system.

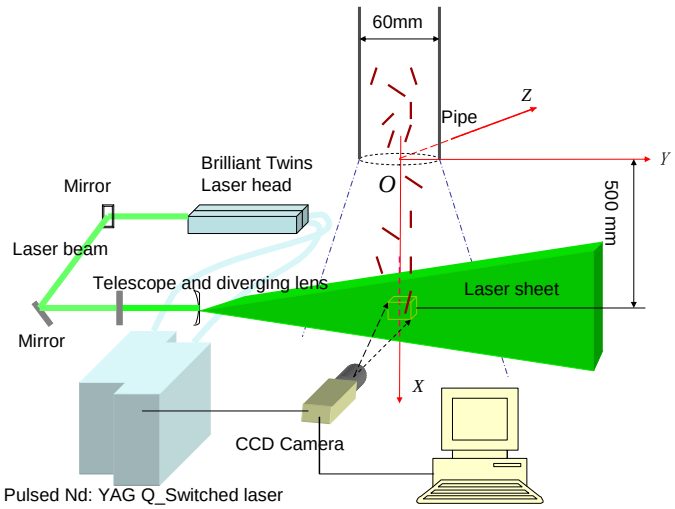

Fig. 1 Experimental arrangement (not to scale). The surrounding settling chamber (650mm×620mm cross section) is not shown for clarity.

The settling chamber was of nominally square cross section with a 650mm × 620mm, height of 2,000mm and was made of Perspex. The fibrous particles were introduced into the top of the chamber and settled over a distance of 2.5-3.0m through a 2,000 mm long pipe of 60mm diameter. Not only did this ensure sufficient length to reach their terminal settling velocities before entering the chamber, it also ensured that any background currents induced by the particles in the chamber were negligible. With a volume fraction of order of 10^{-5}, and cross sectional area of the "jet" of falling particles to the chamber of the order 10^{-2}, any induced chamber flows will be at most 1% that of the particles, which is within experimental error. This neglect ensured the dilute phase was not influenced by any chamber currents in contrast to previous investigation [16]. Also fibres settling velocities were measured for settling distances of both 2.5m and 3.0m. The mean settling velocities obtained were identical for both cases, confirming that the fibres have reached their terminal settling velocities and steady state conditions.

The particle delivering system is axisymmetric, which this greatly facilitates the

measurement, because the measurement can be performed at any vertical plane through the centre line of the pipe. The system can also accommodate spherical particles under identical conditions. This allows direct comparisons to be performed between spherical particles and fibrous particles.

The intensity distribution of laser sheet is nearly Gaussian, as shown in Fig. 7. This property is exploited to determine whether a fibre is fully or partly within the light sheet, as described below. The thickness of the laser sheet was chosen to be around 5mm to provide good illumination of entire particles.

2.2. Property of the fibres

The particles used in the experiments are nylon fibres whose properties are shown in Table 1. A micrograph of a sample of the fibres is shown in Fig. 2, at a resolution of 18 μm/pixel. It can be seen that they are of constant diameter and, while many are straight, a significant number have a slight bend.

Table 1 Nylon fibre used in the experiments

Length, L, μm	2,000
Diameter, d, μm	49.6
Density, ρ_{fp}, kg/m^3	1,150
Aspect ratio, L/d	40
Material	Nylon
Denier	20

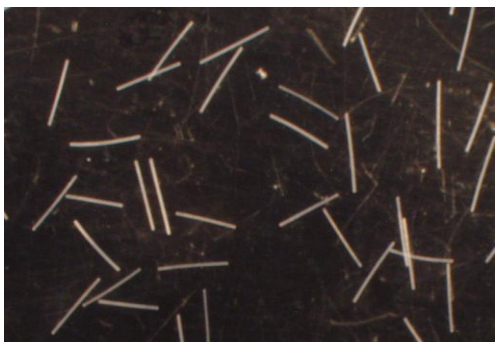

Fig. 2 A micrograph of the sample of nylon fibres.

The length of each fibrous particle (i.e. the major axis) is defined as the maximum distance between any two pixels in the object. This distance is measured from an optical image converted to binary form (see Fig. 3). The minor axis is defined to be perpendicular to the major axis and the rectangle defined by the two axes can enclose the perimeter of the region. This rectangle we call the "basic rectangle" (Gonzalez *et al* [7]). The concept of a basic rectangle can also be used to define fibrous particle's straightness, as shown in Eq. (7).

$$\varepsilon = 1 - \frac{\delta - d_i}{L_i} \qquad (7)$$

where ε is straightness of a fibrous particle; δ is minor axis of the basic rectangle on a binary image; d_i and L_i is the diameter and length of the fibre respectively on the binary image and the subscript " *i* " refers to "image". If a fibre's straightness tends toward unity, the fibre approaches being straight.

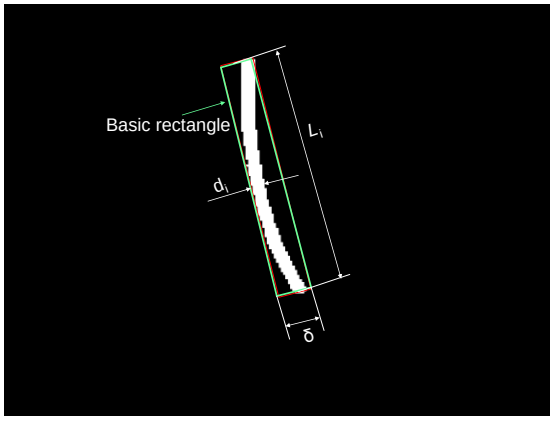

Fig. 3 A binary image of a fibre and its "basic rectangle" used to define its characteristic dimensions.

Fig. 4 presents the distribution of the straightness of the fibrous particles based on a sample size of 1,139. It can be seen that 90.1% of these fibres have straightness $\varepsilon > 0.85$ and some 38% are perfectly straight.

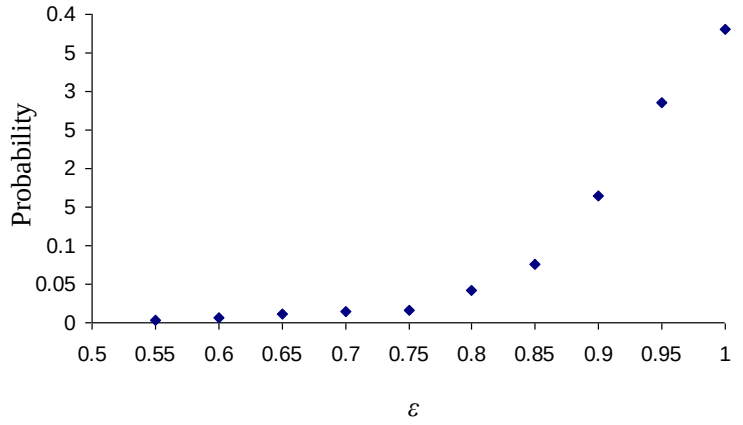

Fig. 4 The distribution of straightness, ε (see Eq. 7) for the present fibres.

Fig. 5 presents the distribution of the fibres length, L, which were measured directly from the two endpoints. It can be seen that 82% of fibres have a length between 1900 and 2100 μm and over 95% between 1800 and 2200 μm, with a standard deviation of 196μm.

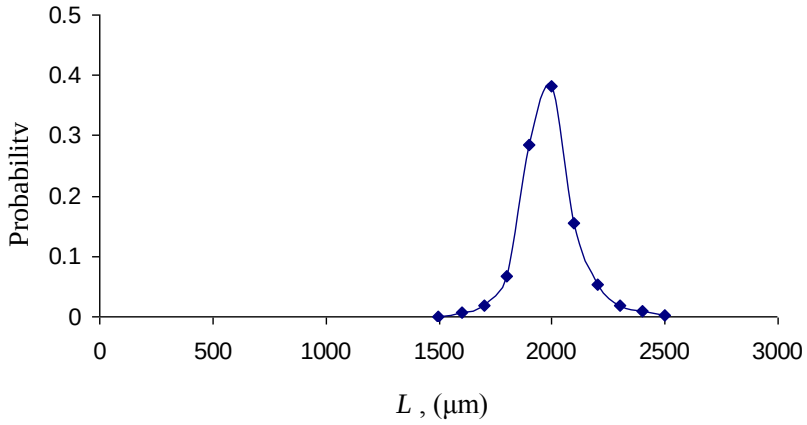

Fig. 5 The distribution of the length, L, of the present fibres.

2.3 Number density, orientation and velocity measurement

Fig. 6 presents the orientation definition of a fibre. The plane of x-y is image plane. The angle of α is defined to be azimuth of a fibre and θ the orientation of a fibre.

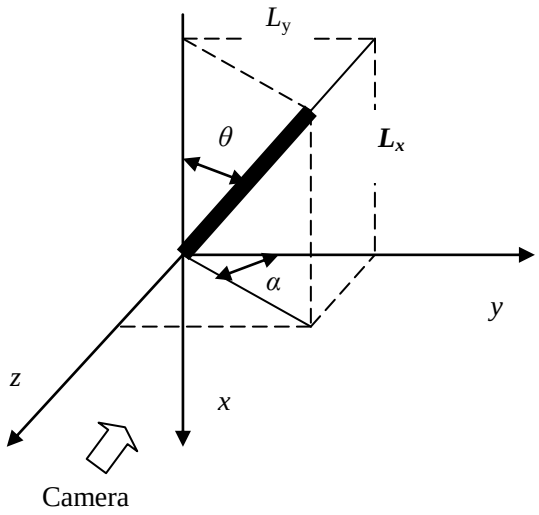

Fig. 6 The definition fibre orientation, where *x*-*y* is image plane

In the present study, we define the volume fraction of fibrous particles as:

$$\phi = \frac{n_p \pi (d/2)^2 L}{1008 \times 1018 R^2 H} \qquad (8)$$

where n_p is the number of fibrous particles in viewing volume, R is the magnification of camera image system, H is the thickness of laser sheet and $1008\times1018R^2H$ is the viewing volume.

In the present experiments of measuring settling velocity and Φ, the volume fraction were controlled to be in the range of $\Phi \leq 0.0001$, which is a super dilute condition so that there were few particles which exhibited clumping. Hence the number density of fibrous particle in the viewing area (volume) was calculated by counting the number of particles, and the volume fraction was computed exactly. The volume fractions were also binned by the number of particles to obtain statistically the influence of particle number density on the fibres' aerodynamic behaviour.

The coordinates of two endpoints of each object (fibrous particle) were obtained. Since the

length L of these fibres is constant, the spatial orientation θ (the angle between the X axis and the major axis of the fibrous particle) of fibres was calculated by following trigonometric function (Fig. 6 and 7):

$$\theta = (\arccos \frac{|x_{e2} - x_{e1}|R}{L}) \times (\frac{180}{\pi}) \quad (°) \qquad (9)$$

where x_{e2} and x_{e1} are coordinates of X values of two endpoints.

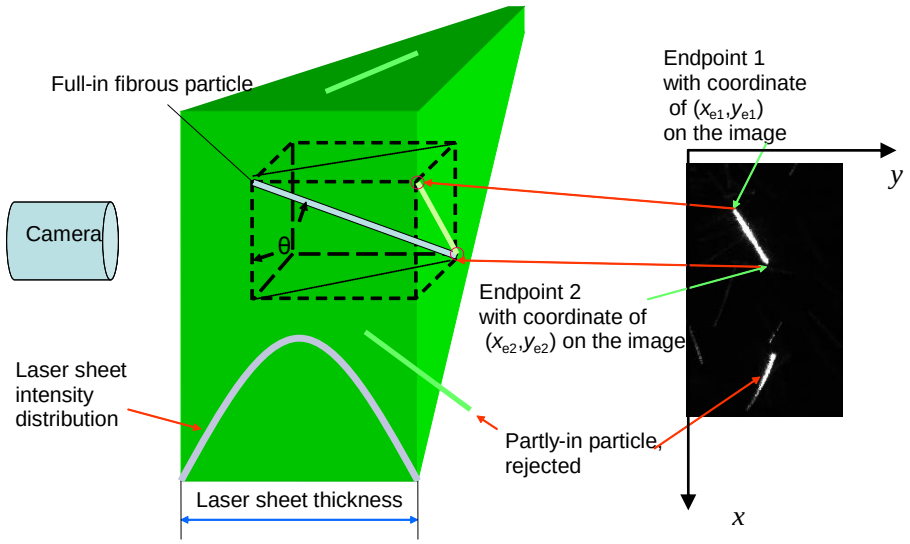

Fig. 7 Schematic diagram of the orientation measurement, the detection of "part-in" fibres and key notation.

Any fibres that are only partly in the laser sheet will give a false calculation of the projected length and the coordinates of endpoints, so must be rejected. This can be achieved by comparing the intensities of the signal at two endpoints of the fibre. Because of the Gaussian light sheet intensity distribution a partly-in fibrous particle will exhibit a significant difference between the intensity values of the two endpoints (Fig. 7). This is used to reject such particles as described in the appendix.

The coordinate system used in the calculation is Cartesian, with the x axis directed

downwards in the direction of gravity. We define the two endpoint velocities of the fibrous particle as $\boldsymbol{V}_{e1}$ and $\boldsymbol{V}_{e2}$. Each endpoint velocity has three components $\boldsymbol{V}_{e1x}$, $\boldsymbol{V}_{e1y}$, $\boldsymbol{V}_{e1z}$ and $\boldsymbol{V}_{e2x}$, $\boldsymbol{V}_{e2y}$, $\boldsymbol{V}_{e2z}$, as shown in Fig. 8 and Eq. (10).

$$\begin{aligned} \vec{V}_{e1} &= \vec{V}_{e1x} + \vec{V}_{e1y} + \vec{V}_{e1z} \\ \vec{V}_{e2} &= \vec{V}_{e2x} + \vec{V}_{e2y} + \vec{V}_{e2z} \end{aligned} \qquad (10)$$

Based on Eq. (10), we define V_{e1x} and V_{e2x} as vertical components of the settling velocity of the endpoints 1 and 2 respectively of the fibrous particle. Similarly V_{e1y} and V_{e2y} are the horizontal components of settling velocity of endpoints 1 and 2 of the fibrous particle respectively.

Image pairs were recoded by the digital camera with a known time separation (Δt). After image processing the displacements of two endpoints of fibrous particles along the x and y axis can be obtained. From this $\boldsymbol{V}_{e1x}$, $\boldsymbol{V}_{e1y}$ and $\boldsymbol{V}_{e2x}$, $\boldsymbol{V}_{e2y}$ can be calculated by Eq. (11), as follows:

$$V_{e1x} = \frac{(x_{e12} - x_{e11})R}{\Delta t}, V_{e1y} = \frac{(y_{e12} - y_{e11})R}{\Delta t}, V_{e2x} = \frac{(x_{e22} - x_{e21})R}{\Delta t}, V_{e2y} = \frac{(y_{e22} - y_{e21})R}{\Delta t} \qquad (11)$$

where V_{e1x} is the velocity of endpoint 1 in the x direction; V_{e1y} is the velocity of endpoint 1 in the y direction; V_{e2x} is the velocity of endpoint 2 in the x direction; V_{e2y} is the velocity of endpoint 2 in the y direction; x_{e12} is x axis coordinate of endpoint 1from the second image, x_{e11} is x axis coordinate of the endpoint 1from the first image; y_{e12} is y axis coordinate of the endpoint 1 from the second image and so on.

Fig. 8 shows the definition of settling velocity of centroid of a fibrous particle. The velocity of the centroid of a fibre V_c is defined by Eq. (12):

$$\vec{V}_c = \vec{V}_{cx} + \vec{V}_{cy} + \vec{V}_{cz}$$
$$V_{cx} = \frac{1}{2}(V_{e1x} + V_{e2x})$$
$$V_{cy} = \frac{1}{2}(V_{e1y} + V_{e2y}) \qquad (12)$$
$$V_{cz} = \frac{1}{2}(V_{e1z} + V_{e2z})$$

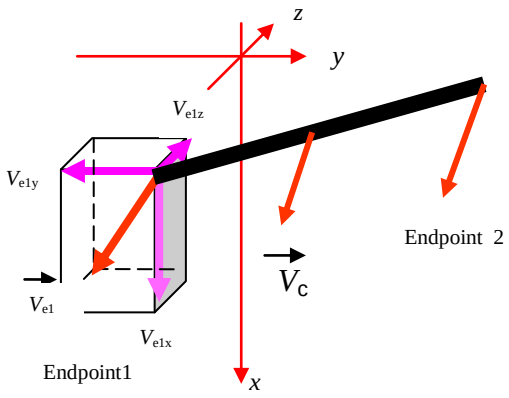

Fig. 8 Two endpoint and centroid velocities of a fibre.

In present study, V_{cx} and V_{cy} represent vertical and horizontal components of settling velocities of a fibrous particle respectively. Because the particle delivery system is vertical and axisymmetric, the distributions of V_{cy} and V_{cz} is identical and V_{cy} is representative. So V_{cz} is ignored.

Since data are obtained from an image pair, the orientation of a fibrous particle equals the average orientation of the fibre from the first and second images:

$$\theta = \frac{1}{2}(\theta_1 + \theta_2) \qquad (13)$$

$$\theta_1 = \arccos \frac{|x_{e21} - x_{e11}|R}{L} \times (\frac{180^\circ}{\pi}) \qquad (14)$$

$$\theta_2 = \arccos \frac{|x_{e22} - x_{e12}|R}{L} \times (\frac{180^\circ}{\pi}) \qquad (15)$$

3 Experimental results and discussions

3.1 Distribution of fibre's settling velocity and orientation

Fig. 9 presents distribution of vertical settling velocity obtained from 29,364 samples for volume fraction less than 5×10^{-4} and Herzhaft and Guazzelli's work [16]. It can be seen the distribution is Gaussian. Fig. 9 indicates that the relatively small size of the error bars shows that the variation in straightness of the fibres does not have a large influence on the settling velocity of these fibres. Furthermore, the absence of any bimodality in the curve implies that there is no fundamental difference in the aerodynamics of perfectly straight and slight curve fibres under the conditions assessed here. That is the presence of a slight curve may increase the scatter in the velocity distribution but does not result in any fundamental change in aerodynamic behaviour, since some fibres are perfectly straight. Finally the significantly lower spread in V_{cx}/V_{ts} compared with the measurements of Herzhaft and Guazzelli[16], who did use perfectly straight fibres, suggests that the influence of volume fraction is more significant than that of straightness.

Fig. 10 shows the orientation distribution of fibrous particles obtained from 29,364 samples over the range of a volume fraction, $\Phi < 5\times10^{-4}$. It can be seen the majority of fibres are broadly, but not exactly, horizontal. This agrees with Fan *et al* [1] and Clift *et al* [2].

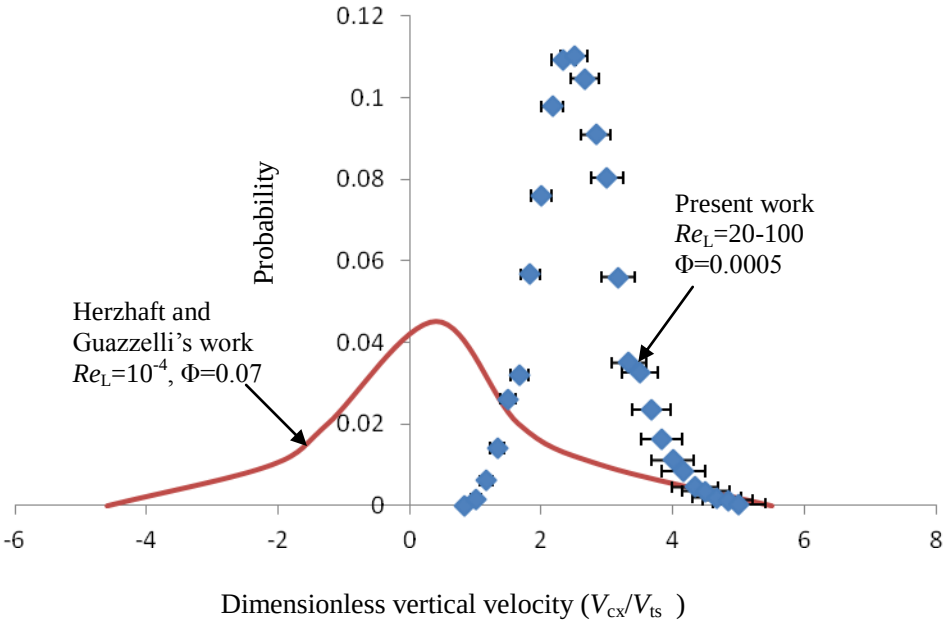

Fig.9 The measured distribution of settling velocity V_{cx} relatively to the terminal velocity of an isolated particle, V_{ts}, at volume fraction $\Phi < 5\times10^{-4}$

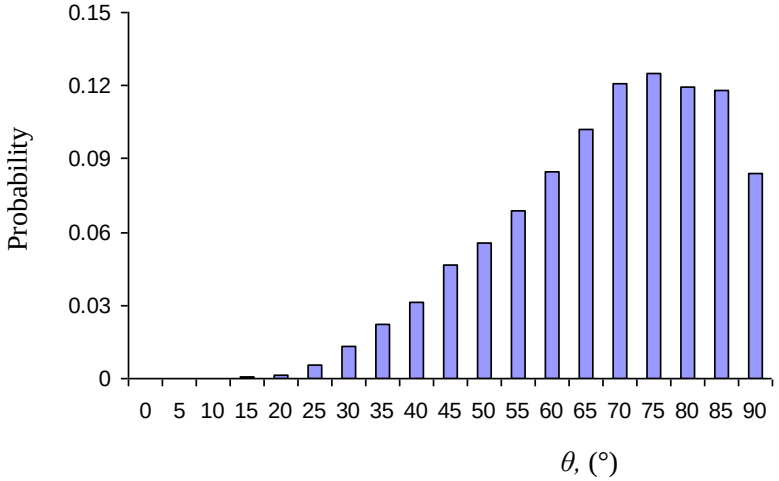

Fig. 10 The measured distribution of the orientation of present fibres from the vertical, at volume fraction $\Phi < 5\times10^{-4}$

3.2 Influences of volume fraction on vertical component of settling velocity of fibrous particles

Fig. 11 presents the relationship between volume fraction (Φ) and the mean vertical component of settling velocity ($\overline{V_{cx}}$) under the condition of low number density (0.1×10^{-5} – 10×10^{-5}). The measurements conducted in super dilute condition. Thousands of runs were performed and per volume fraction were sorted out by image processing. The data point corresponding to the lowest volume fraction in Fig. 11 represents the case of one isolated particle per image and highest volume fraction is 98 fibres per image. Each data point of $\overline{V_{cx}}, \overline{\theta}$ and $\overline{V_{cy}}$ comes from the average of per volume fraction which has hundreds of data in Fig.11-13. It can be seen that $\overline{V_{cx}}$ increases monotonically with Φ. Furthermore the scatter in the data also increases with Φ, the RMS of the data has a similar trend. Eq. (16) is proposed to describe relationship between the number density and the vertical component of settling velocity for the dilute regime.

$$\frac{\overline{V}_{cx}(\phi)}{\overline{V}_{ts}} = a\phi^{n} \qquad (16)$$

where $\overline{V_{ts}}$ is average terminal settling velocity of a single fibre; a and n are constants that are expected to depend on fibre's aspect ratio and Reynolds number; The constants in Eq. (16) for the present fibres are: $\overline{V_{ts}}$ =0.375, a=7.310 and n=0.1519. That is

$$\overline{V}_{cx}(\phi) = 2.743\phi^{0.1519} \qquad (17)$$

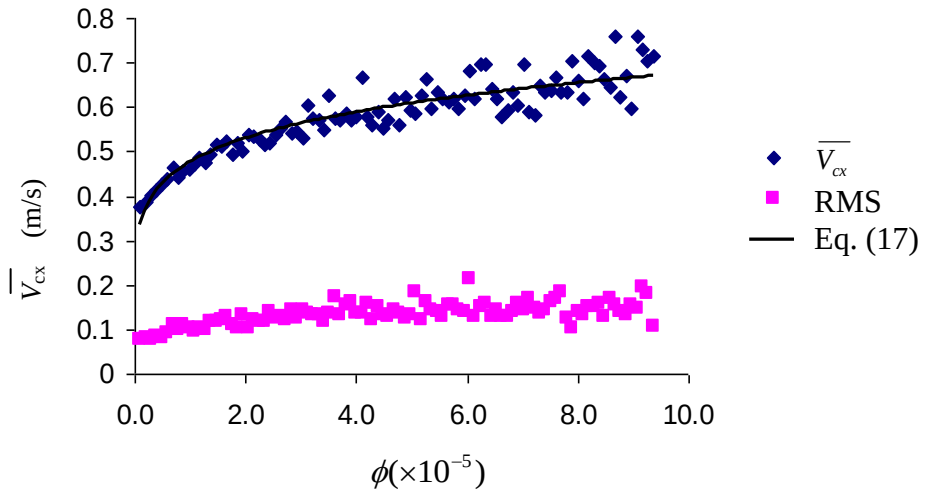

Fig.11 The relationships between Φ and $\overline{V_{cx}}$ for fibrous particles settling in air

The data point corresponding to the lowest volume fraction in Fig. 11 represents the minimum of $\overline{V_{cx}}$ (terminal settling velocity of an isolated fibre), with all other values of $\overline{V_{cx}}$ exceeding it in Φ=0.1× 10^{-5} – 10 × 10^{-5} regime.

3.3 Influences of volume fraction on orientation of fibrous particles

Fig. 12 presents the relationship between the Φ and mean orientation ($\bar{\theta}$). It can be seen $\bar{\theta}$ decreases with Φ, i.e. the fibrous particles tend to become more horizontal with decreasing Φ. These data can also be described by a power relationship:

$$\bar{\theta}(\phi) = \frac{b}{\phi^n}\bar{\theta}_{ts} \quad (°) \qquad (18)$$

where b is a constant and $\overline{\theta_{ts}}$ is average orientation of a single fibre when settling in air. In the above case, $\overline{\theta_{ts}}$ =81.38° and n=0.0654, b=0.428. This result can explain why the value of $\overline{V_{cx}}$ increases with the increasing of Φ. An increase in Φ causes the fibre's major axis to

tend to be more vertical, causing $\overline{V_{cx}}$ to increase, due to increased aerodynamic interaction between particles.

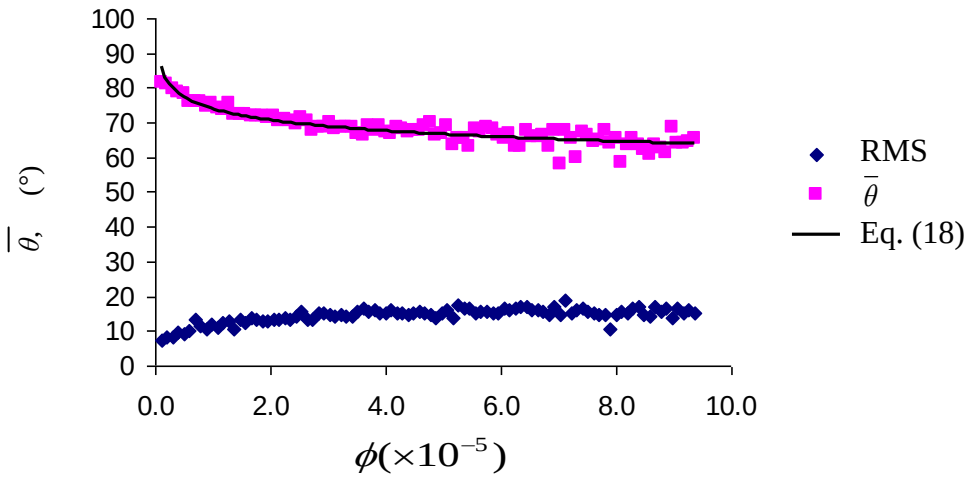

Fig. 12 The relationship between $\overline{\theta}$ and Φ

3.4 Influences of volume fraction on horizontal component of settling velocity of fibrous particles

Fig. 13 presents the relationship between mean horizontal component of settling velocity $\overline{V_{cy}}$ and Φ. It can be seen that $\overline{V_{cy}}$ is zero on average and the fluctuation of $\overline{V_{cy}}$ increases monotonically with Φ. The RMS is well characterized by a power law as follows:

$$\text{RMS of } \overline{V_{cy}} = 0.0167\ \Phi^{0.2495} \qquad (19)$$

The fluctuation of $\overline{V_{cy}}$ values indicates the trajectories of settling fibres are not straight line. The aerodynamic interaction increases the absolute value of $\overline{V_{cy}}$.

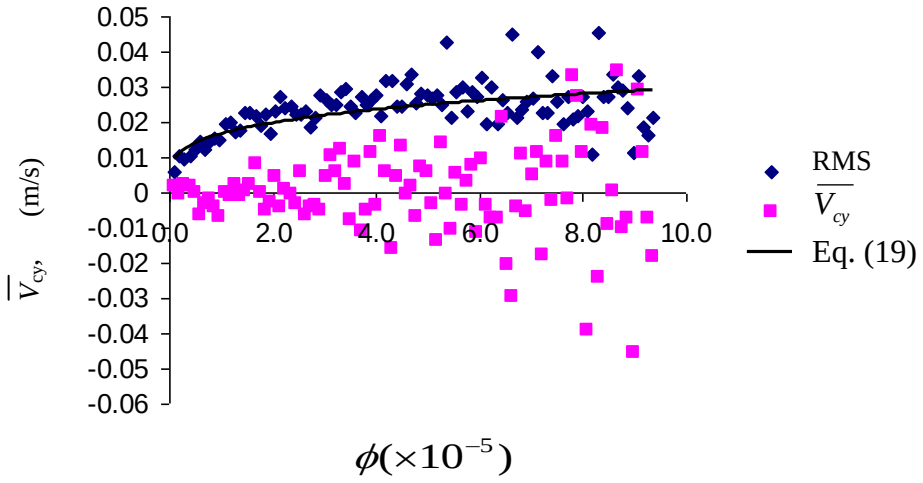

Fig. 13 The relationship between $\overline{V_{cy}}$ and Φ

3.5 Assessment of characteristic length of a fibre when settling in air

The definition of the Reynolds number of a settling fibrous particle in air requires a characteristic length scale. The *Re* of a fibre can be calculated using diameter *d*, length *L* or equivalent d_{eq}. Assuming that an equivalent "diameter" d_{eq} can be found, it is possible to define a Reynolds number Re_{eq} of a single fibre as follows:

$$\mathrm{Re}_{eq} = \frac{\rho_{air} V_{ts} d_{eq}}{\mu} \qquad (20)$$

When settling in air, the fibre's drag force can then be defined as follows:

$$F_D = \frac{1}{2}\rho_{air} C_D V_{ts}^{\ 2} A_{eq} = \frac{1}{2}\rho_{air} C_D V_{ts}^{\ 2} \pi (\frac{d_{eq}}{2})^2 \qquad (21)$$

The force due to gravity is $F_g = \rho_{fp}\pi(\frac{d}{2})^2 Lg$, and when the fibre reaches its terminal settling velocity $F_g = F_D$:

$$\rho_{fp}\pi(\frac{d}{2})^2 Lg = \frac{1}{2}\rho_{air} C_D V_{ts}^{\ 2} \pi (\frac{d_{eq}}{2})^2 \qquad (22)$$

combining Eqs. (20) and (22) gives $C_{\mathrm{D}}(Re_{\mathrm{eq}})^2$:

$$C_D(\mathrm{Re}_{eq})^2 = \frac{2\rho_{fp}\rho_{air}d^2Lg}{\mu^2} = K \quad (23)$$

In Eq. (23), K is a constant for a given fibre, so we can obtain relationship of present fibre between C_D and $(Re_{eq})^{-2}$ theoretically, as shown in Fig. 14:

$$C_D = K(\mathrm{Re}_{eq})^{-2} = 412.81(\mathrm{Re}_{eq})^{-2} \quad (24)$$

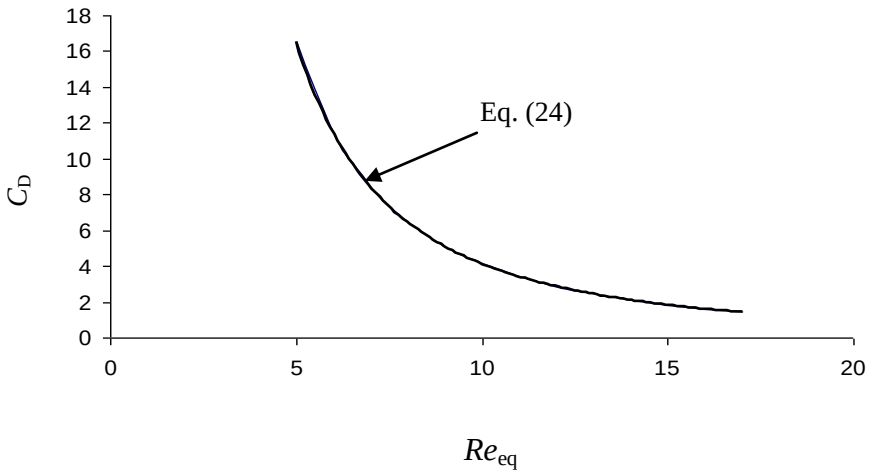

Fig. 14 The theoretical relationship between Re_{eq} and C_D

If we define d_{eq} based on the fibre's projected area, in the vertical direction it is:

$$A_{eq} = \pi(\frac{d_{eq}}{2})^2 = dL\sin\theta + \pi(\frac{d}{2})^2\cos\theta \quad (25)$$

We can experimentally measured C_D from Eq. (26):

$$C_D = \frac{F_D}{\frac{1}{2}\rho_{air}V_{ts}{}^2A_{eq}} = \frac{\rho_{fp}\pi(\frac{d}{2})^2Lg}{\frac{1}{2}\rho_{air}V_{ts}{}^2(dL\sin\theta + \pi(\frac{d}{2})^2\cos\theta)} \quad (26)$$

Meanwhile $\mathrm{Re}_d = \frac{\rho_{air}V_{ts}d}{\mu}$, combining Eq (26) and gives:

$$C_D = \frac{\rho_{air}\rho_{fp}\pi d^3Lg}{2\,\mathrm{Re}_d{}^2\,\mu^2(L\sin\theta + \frac{1}{4}\pi d\cos\theta)} \quad (27)$$

Eq. (27) is relationship between C_D and Re_d and orientation θ.

Fig. 15 presents the experimental relationship between Re and C_D based on 94 single settling fibres and the Re were calculated using the fibre's diameter d, length L, volume equivalent diameter d_{ev} and surface equivalent diameter d_{es} respectively. We plot $C_D - Re$ (Eq.26 and 20) by changing d_{eq} until the curve of Fig. 15 coincides Fig. 14, then we obtained d_{eq} = 354μm for present fibre, see Fig. 16. After that Eq. (25) becomes:

$$396800.00\sin\theta + 7728.82\cos\theta = 393691.82 \qquad (28)$$

Solving Eq. (28), we can obtain θ_{eq} = 81.62°. Comparing with Eq. (18), $\overline{\theta_{ts}}$ =81.38° it can be seen that average orientation of a settling single fibre can be used in Eqs. (25), (26). Therefore from Eq. (25) the equivalent "diameter" d_{eq} of a fibre settling in air is as follows:

$$d_{eq} = \sqrt{\frac{4Ld\sin\overline{\theta}_{ts}}{\pi} + d^2\cos\overline{\theta_{ts}}} \qquad (29)$$

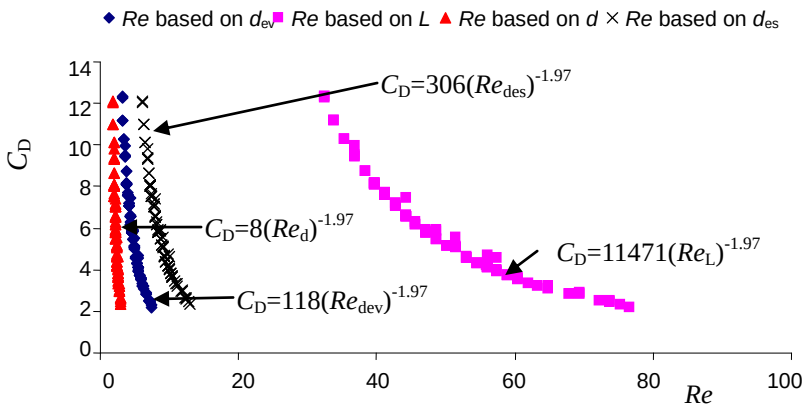

Fig. 15 The experimental dependence of drag coefficient on Reynolds number based on length $Re_{L,}$ on diameter Re_d, on equivalent surface area diameter Re_{des} and on equivalent volume diameter Re_{dev}

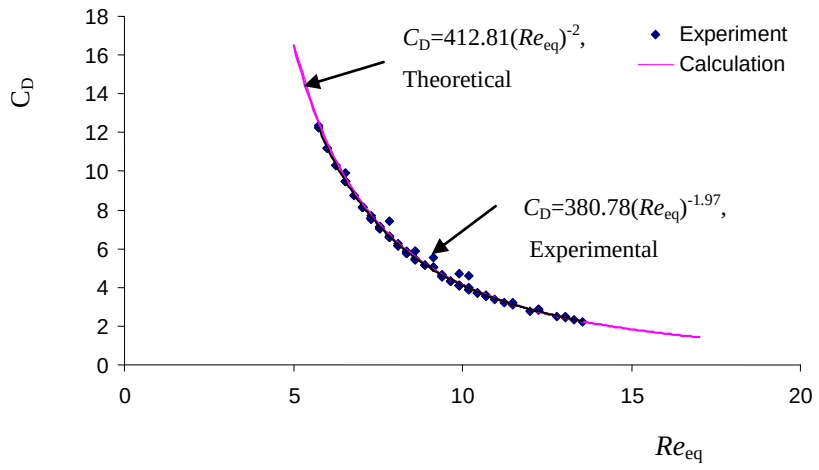

Fig. 16 Theoretical and experimental relationship between C_D and Re_{eq}, where d_{eq} is defined in Eq. (29)

The models proposed by Fan *et al* [1] and Clift *et a*l [2] are based on diameter, *d*, of the fibre. Hence we use this characteristic length to assess their models in Fig. 17. From the figure we can see that these models do not describe the behaviour of present particles. For Fan's model, as can be seen from Eq. (1), the term of $(\frac{\rho_{fp}}{\rho_f})^{-1.537}$ plays an important role when ρ_{fp} is far greater than ρ_f. For present case $\rho_{fp} / \rho_f = 958$, it predicts C_D far less than the present values. Hence their model is poorly suited to fibre-gas two-phase flow. For Clift's model $C_D = 9.689(\mathrm{Re}_d)^{-0.78} + 1.42(\mathrm{Re}_d)^{0.04}$ ($0.1 < Re_d < 5$), the power of -0.78 is far greater than -2, so its slope is much lower than that of present fibres. As mentioned in section 3.1, the presence of slight curve of fibres increase the scatter in settling velocity distribution, this can cause a bias on C_D. However no comparable data is available against which to provide a quantitative assessment of the effect.

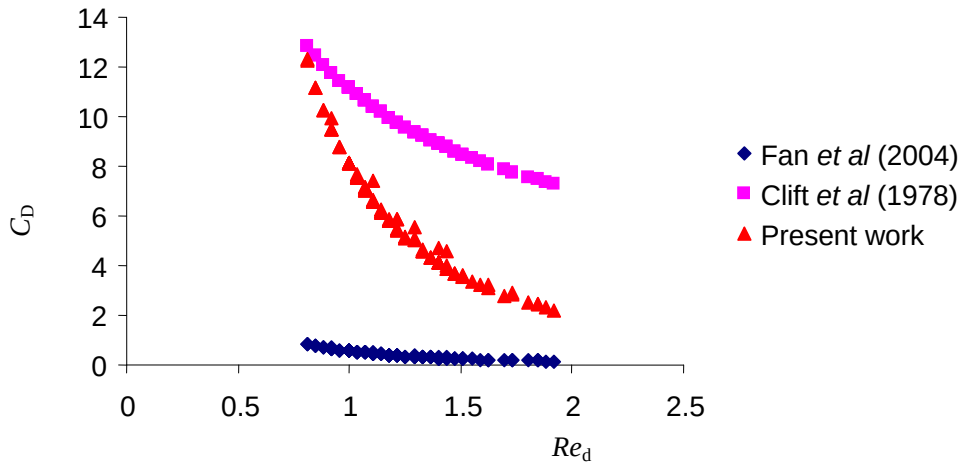

Fig. 17 The relationship of Re_d and C_D between present and Fan's and Clift's work

4 Conclusions

In this work, we measured the vertical and horizontal components of settling velocities, orientation and number density for long fibres settling in air with $Re \sim O(1)$ and for volume fractions $\Phi = 10^{-6}$ - 5×10^{-4}. The mean vertical settling velocities were found to increase monotonically with Φ. The mean orientations decrease with Φ. We show that all the mean steady state settling velocities of multiple fibres exceed the mean terminal settling velocity of a single fibre under $\Phi < 10^{-4}$. This phenomenon is attributed to fibres' orientation transition from horizontal state to vertical under super dilute regime that stems from increasing aerodynamic interactions between fibres. The mean horizontal settling velocity was zero on average. However the fluctuations of the horizontal components of settling velocities of settling fibres were found to increase with volume fraction. Finally the controlling length scale in the relationship between Reynolds number and drag coefficient was assessed. It is found that the diameter based on the projected area with mean orientation describes the relationship well, while all other length scales fail. The models of Fan *et al* [1] and Clift *et al* [2] were also found to be in poor agreement with present measurements.

Acknowledgement

This study has been supported by the Faculty of Engineering, Computer & Mathematical Science of The University of Adelaide and by an ARC Discovery Grant, both of which are gratefully acknowledged.

References

[1] L. Fan, Z. Mao, C. Yang, Experiment on Settling of Slender Particles with Large Aspect Ratio and Correlation of the Drag Coefficient, Ind. Eng. Chem. Res. 43 (2004), pp7664 - 7670.

[2] R. Clift, J. Grace and M. Weber, Bubbles, drops, and particles, ISBN 0-12-176950-X, Academic Press, New York, 1978

[3] A. Haider and O. Levenspiel, Drag coefficient and terminal velocity of spherical and nonspherical particles, Powder Technology, 58 (1989), pp63-70.

[4] G. Venu Madhav, R. P. Chhabra, Drag on non-spherical particles in viscous fluids, International Journal of Mineral Processing, 43(1995), pp15-29

[5]G. H. Ganser, A rational approach to drag prediction of spherical and nonspherical particles, Powder Technology, 77(1993), pp143-152

[6] P. K. Swamee, C. P. Ojha, Drag coefficients and fall velocity of non-spherical particles J. Hydraul. Eng. 117(1991)

[7] R. Gonzalez, R. Woods, S. Eddins, Digital image processing using Matlab, ISBN 0-13-008519-7, Pearson Education, 2004

[8] R. P. Chhabra, L. Agawal, N. K. Sinha, Drag on non-spherical particles: an evaluation of available methods, Powder Technology, 101(1999), pp288-295

[9] Z. L. Arsenijevic, Z. B. Grbavcic, R. V. Grulovic, F. K. Zdanski, Determination of non-spherical particle terminal velocity using particulate expansion data, Powder Technology,

103 (1999), pp265-273

[10] H. Y. Xie, D. W. Zhang, Stokes shape factor and its application in the measurement of sphericity of non-spherical particles, Powder Technology, 114 (2001). pp102-105

[11] P. Rajitha, R. P. Chhabra, N. E. Sabiri and J. Comiti, Drag on non-spherical particles in power law non-Newtonian media, International Journal of Mineral Processing, 78 (2006), pp110-121

[12] S. Tran-Cong, M. Gay and E. E. Michaelides, Drag coefficient of irregularly shaped particles, Powder Technology, 139(2004), pp21-32

[13] A. Unnikrishnan, R. P. Chhabra, An experimental study of motion of cylinders in Newtonian fluids: wall effects and drag coefficient, the Canadian Journal of Chemical Engineering, Vol. 69, 1991

[14] J. Gabitto and C. Tsouris, Drag coefficient and settling velocity for particles of cylindrical shape, Powder Technology 183 (2008), pp314-322

[15] G. McKay, W. R. Murphy and M. Hillis, Settling characteristics of discs and cylinders, Chem Eng Res Des, Vol. 66, 1988

[16]B. Herzhaft, and E. Guazzelli, Experimental study of sedimentation of dilute and semi-dilute suspensions of fibres, Journal Fluid Mech, Vol 384 (1999) pp133-158

Appendix

Image processing

The purpose of the image processing is to extract measurements for each particle using Eqs. 9-15 and to thus allow the aerodynamic behaviour of the fibrous particle to be assessed statistically under various conditions. From the coordinates of two endpoints it is possible to calculate the orientation and velocities of a fibre.

Those fibrous particles located at the edges of an image yield a false measurement of its length. Therefore first step of image processing is to remove these fibrous particles from the images. The second step is to convert the image into binary form. The third step is to remove small objects. Binary images typically contain “noise” which comprises spurious signal in one or two isolated pixels. They are not real fibrous particles and so need to be removed. The fourth step is to label the fibres. This is a very important and useful step in images processing. By using this tool the background pixels were labeled 0. The pixels that made up the first object were labeled 1, (see Fig. A1) those labeled 2, the second object, and so on. If there were *n* particles in the viewing volume the last pixels (object) would be labeled *n*. Therefore this tool can be used to count the number of fibres in the image exactly.

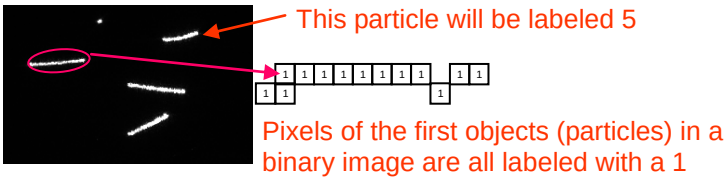

Fig. A1 Step 4--labeling pixels of fibrous particles in a binary image.

The fifth step is removing fibrous particles “partly-in” the laser sheet. As previously noted, the measured lengths of such fibrous particles are false. Therefore these part-in fibres must also be removed from the images when processing. Fig. A2 displays the different characteristics of full-in and part-in fibrous particles. For a “full-in” fibrous particle, the intensity along the major axis of the fibre is nearly constant while for a part-in one, the intensity at the two endpoints differs significantly (Fig. A2). Hence it is possible to discriminate by either comparing the intensity of two endpoints of the fibre, or by comparing the standard deviation of intensity along the major axis. If the standard deviation is less than the threshold, it is a full-in fibrous particle.

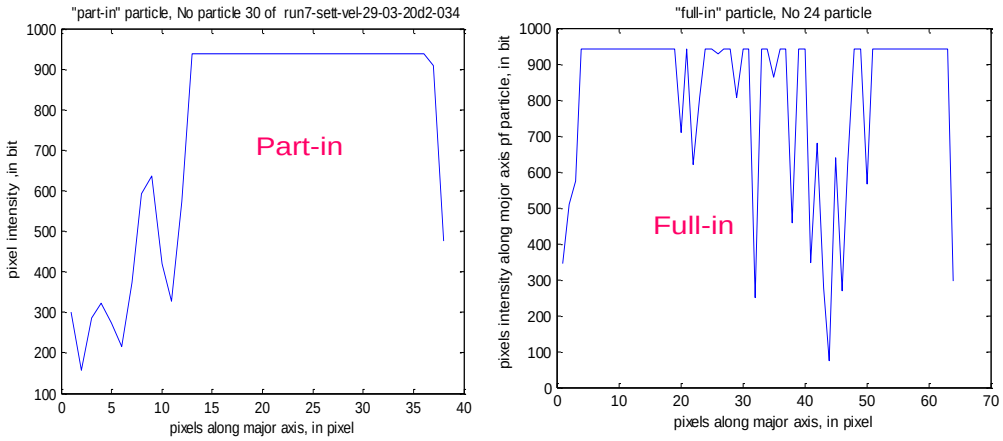

Fig. A2 The distributions of intensity along major axis for part-in and full-in fibrous particles in the laser sheet.

The last step is tracking particles and calculating velocities and orientations. Fig. A3 presents a pair of images of fibres with a known time separation of 2500 μs. The circles highlight those fibrous particles that are pairs. It can be seen that if the time separation is short enough, any changes in fibre's length is small, orientation and area are small. Based on these characteristics on the images, tracking particles (matching pairs) becomes easier than for spherical particles.

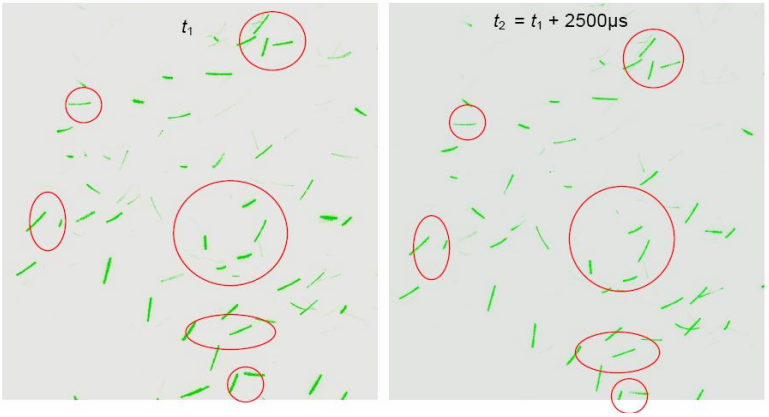

Fig. A3 A pair of images of fibres with a known time separation of 2,500 μs,

sets of obviously matching pairs are encircled.

The accurate matching of pairs of fibrous particles within a known time separation is a most important step in image processing. From this, the vertical and horizontal displacements of each particle can be obtained, and hence the vertical and horizontal components of settling velocities can be calculated. After collecting of the two endpoint's coordinates and matching particle pairs in each pair of images, all components of settling velocities (translational and rotational) of the centroid and orientation of a fibrous particle can be obtained from Eqs. 9-15. The end point of a fibre moves by average 50 pixels, and the total uncertainty in the position of the end point is 4 pixels, then this corresponds to a relative uncertainty in the spatial position of the end point of 8%.